Regional climate model RACMO2

In this study we use output of the Regional Atmospheric Climate MOdel RACMO2 (Van Meijgaard et al. (2008)). RACMO2 combines the physical schemes developed by the European Center for Medium-Range Weather Forecasts (ECMWF, Cycle23r4, White (2001)) and the dynamical core from HIRLAM (Undén et al. (2002)). It is adapted for use over ice sheets, with the recent inclusion of a multi-level snow scheme (Bougamont et al. (2005), Ettema et al. (2010)), which includes a sophisticated snow albedo scheme (Gardner and Sharp (2010)) that is dependent on snow grain size evolution (Flanner and Zender (2006)) and has been extensively validated over Antarctica (Kuipers Munneke et al. (2011)) and Greenland (Van Angelen et al. (2012)). The spatial representation of surface albedo in summer is further improved by using a MODIS-derived background ice albedo (Van Angelen et al. (2012)). Moreover, RACMO2 includes drifting snow physics (Lenaerts et al. (2012a)), and has been successfully applied to studies of the surface mass balance of the Greenland (Ettema et al. (2009)) and Antarctic (Lenaerts et al. (2012b), Kuipers Munneke et al. (2012)) ice sheets.

RACMO2 has 40 vertical atmospheric levels and ∼11 km horizontal resolution. At the lateral boundaries, it is forced by ERA-40 (1960-1978, Uppala et al. (2005)) and ERA-Interim (1979-2011, Dee et al. (2011)) and HADGEM2-ES (1971-2098, The HadGEM2 Development Team (2011)) atmospheric fields at a 6-hourly temporal resolution. Sea ice-cover and sea-surface temperature are prescribed from ERA-40/ERA-Interim/HadGEM2-ES. The domain encompasses a major part of the Arctic, from mainland Canada in the west to Svalbard in the east, and CAA is located far enough from the domain boundaries to prevent model biases related to the interpolation from the ERA-Interim/HADGEM2-forcing data to the true RACMO2 resolution.

In-situ observations

In-situ observations of SMB (Fig. 2), precipitation (Fig. S1A) and near-surface temperature (Fig. S1B) were used for model evaluation. Data are assembled by Gardner et al. (2011), and data sources and further details are available in their supplementary material. Most observational SMB data are collected

along transects, and the distance between neighboring measurements is often small (a few kilometers). However, the various measurement locations have different missing years; i.e., the values shown in Fig. 2A represent spatial as well as temporal SMB variability.

Fig. 2 shows that RACMO2 is able to resolve the spatial and temporal SMB variability on all glaciers, except for Meighen Ice Cap, a small (75 km^2), low-lying and shallow ($\sim$200 m) ice cap on a remote island west of Axel Heiberg Island (Fig. 2A). The presence of ice here has been ascribed to the frequent occurrence of fog above the ice cap (Alt (1979)), preventing sunlight to penetrate to the ice surface. This local phenomenon is not captured by RACMO2 and SMB is therefore largely underestimated, but due to the limited volume of Meighen Ice Cap, this does not significantly affect NCAA mass change.

GRACE

GRACE solutions are retrieved following the technique of Wouters et al. (2008) using the GRACE RL05 data processed by the Center for Space Research (Austin, TX, USA). It uses a forward model to recover the mass balance in five CAA basins (Gardner et al. (2011)). The mass distribution is estimated using an iterative method, which minimizes the root mean square difference between model and observations. To correct for potential biases from near-by areas (e.g. western Greenland), mass changes are simultaneously estimated in the neighboring regions. Corrections are applied to account for the (small) solid earth contributions caused by glacial isostatic adjustment.

Glacier hypsometry

The original ice-covered area in RACMO2 was too large compared to observations, both in NCAA and SCAA. Therefore, the ice mask has been adapted. Based on the glacier outlines from Gardner et al. (2011), we decreased the size of the glacierized area in NCAA and SCAA to 105000 and 40800 km^2, respectively (Fig. S2). Hypsometries from RACMO2 are compared with high-resolution DEM hypsometry for the ice-covered areas in NCAA and SCAA (Fig. S2). Although hypsometry is generally well represented by RACMO2, the extent of the area that is located below 1000 m is overestimated. Therefore, we corrected

the modeled SMB by redistributing the SMB according to the DEM classes, and used the corrected SMB in the interpretation of the results. Generally, the SMB bias due to hypsometry differences is small ($\sim$10 Gt yr^{-1}), but is found to increase throughout the 21st century (to $\sim$15 Gt yr^{-1}), when SMB becomes increasingly negative.

Present-day SMB uncertainties

In Fig. 3, RACMO2 cumulative mass anomalies are plotted with respect to the start of the simulation (1960). The SMB uncertainty is calculated as the sum of squared errors in accumulation and meltwater runoff, and is accumulated over all months in the period 1960-2011. Since according to RACMO2 surface sublimation and drifting snow processes are negligible ($<$1 Gt yr^{-1}) in CAA, the relative error in accumulation is assumed to be equal to the model bias in precipitation (10%, Fig. S1A). The uncertainty in meltwater runoff is assumed equal to the mean bias in mass loss in the summer (JJA) in RACMO2 compared to GRACE (2003-2011), i.e. 28% for NCAA and 34% for SCAA. Note that meltwater runoff from the tundra is included in this estimate.

SMB uncertainties in the 21st century

The model sensitivity to feedbacks which are known to affect the surface mass balance, but (which are) not explicitly included in this study, is estimated with simple sensitivity tests. Two feedbacks are considered: firstly, due to glacier melt, the ice cap edges will retreat, which leads to a decrease in mass loss. Here we consider, 1, 5 and 10% loss in glacier area along the edges, linearly increasing with time. Secondly, due to ice melt, the elevation decreases at an annual rate that is equivalent to the SMB (assuming ρ_{ice} to be equal to 917 kg m^{-3}). On the ice cap edges, where melt is strong, thinning of $>$100 m is predicted at the end of the 21st century, whereas cumulative thickening of $>$10 m occurs in the accumulation area. Fig. S3 shows the effect on the surface mass balance in the 21st century (10-50 Gt yr^{-1}). Especially local thinning strongly decreases surface mass balance, particularly in SCAA, potentially doubling total volume loss of SCAA at the end of the 21st century. The reason is that in SCAA, the SMB-elevation

gradient is very steep in the ablation zone, making this region extremely sensitive to the positive feedback between thinning and melt. However, since we neglect the effects of ice flow, the impact of both feedbacks is probably exaggerated. A full assessment would require ice-dynamical modeling of all CAA glaciers, which is beyond the scope of this study.

HadGEM2-ES General Circulation Model

For the 21st century, RACMO2 was forced with output from HadGEM2-ES, a fully-coupled CMIP5 General Circulation Model (GCM). HadGEM2-ES includes all atmospheric, oceanic and terrestrial components, including land and sea ice physics (The HadGEM2 Development Team (2011)). The historical simulation of HadGEM2-ES (1971-2004) is driven by observed CO_2 concentrations. Within the CMIP5-model ensemble, it performs reasonably well in simulating present-day general circulation in the Arctic. Present-day sea ice cover in Baffin Bay and Nares Strait is somewhat overestimated (Fig. S4), especially along the CAA coast. The HadGEM2-scenario run (2005-2098) is driven by the moderate RCP4.5 scenario (Moss et al. (2010)). This scenario projects an enhanced radiative forcing in the 21st century, increasing from 2 $\mathrm{W\,m^{-2}}$ in 2005 to 4.5 $\mathrm{W\,m^{-2}}$ in 2070, stabilizing afterwards. Table 1 shows that SMB in the RACMO2 control simulation with the HadGEM2-ES forcing (1971-2000) is more negative than the ERA-Interim forced simulation (-58 vs. -13 $\mathrm{Gt\,yr^{-1}}$), due to underestimated precipitation in NCAA (-7 $\mathrm{Gt\,yr^{-1}}$, 25%) and higher runoff, also mainly in NCAA (+28 $\mathrm{Gt\,yr^{-1}}$, 90%), and to a lesser extent in SCAA (+10 $\mathrm{Gt\,yr^{-1}}$, 25%). The latter is associated with overestimated near-surface temperatures ($\sim$1 K) in the high Arctic. The GCM-forced RACMO2 SMB (1971-2000) is however similar to the 2000-2011 SMB of the ERA-Interim forced run (-58 vs. -48 $\mathrm{Gt\,yr^{-1}}$), implying that the temperature forcing from the GCM is typical for the recent (warm) Arctic climate. The underestimated precipitation in NCAA may be related to overestimated sea-ice extent along the CAA coast in HadGEM2-ES (Fig. S4).

AR5 multi-model and multi-scenario ensemble

To put our results in a broader perspective, we compared the temperature evolution in the HadGEM2-ES model forced by the RCP4.5 scenario with the other AR5 models for all scenarios (RCP2.6, RCP4.5 and RCP8.5). In total, output from 76 different simulations and 94 consecutive years (2005-2098) is used, which represents ∼7000 realisations in total. HadGEM2-ES summer (JJA) near-surface warming in the 21st century is similar to the AR5 RCP4.5 multi-model mean (2.3 K) and somewhat lower than the average of all multi-model scenarios (2.9 K).

The estimated sensitivity of CAA SMB to near-surface temperature, which is averaged over 60-84°N, 60-110°W and taken directly from HadGEM2-ES, is -36±3 $\mathrm{Gt\,K^{-1}\,yr^{-1}}$. Although this relation may be sensitive to the choice of GCM (Fettweis et al. (2012)), it agrees within the uncertainty bounds with the sensitivity that originates from the ERA-reanalysis data (1960-2011, -29±4 $\mathrm{Gt\,K^{-1}\,yr^{-1}}$). This estimated sensitivity is clearly lower than the sensitivity found by Gardner et al. (2011) (-64 ± 14 $\mathrm{Gt\,K^{-1}\,yr^{-1}}$). The reason is that Gardner et al. (2011) only included glaciated surfaces, where the summer air temperatures cannot reach far above the melting point; hence temporal variability of summer temperature remains small, and the associated sensitivity to temperature high. Here, we included tundra and ocean surfaces as well, which can heat up more quickly in summer.

This relation can be applied to all AR5 modeled temperature scenarios averaged for the same region in order to calculate the probability distributions of different SMB classes (Fig. 4D). To translate the uncertainty arising from choosing a single AR5 GCM towards an uncertainty estimate of CAA SMB, we calculated the AR5-ensemble variability in near-surface temperature for CAA. We used the standard deviation of all AR5 modeled near-surface summer temperature differences between 1971-2000 and 2080-2098, which equals 1.9 K. The total annual uncertainty therefore equals 67 $\mathrm{Gt\,yr^{-1}}$ (1.9 times the estimated sensitivity of SMB for temperature). This uncertainty was included when calculating the SMB distributions (Fig. 4D). To estimate the uncertainty of 21st century CAA mass loss, this annual uncertainty was accumulated from 2005 to 2098.

References

B. T. Alt. Investigation of summer synoptic climate controls on the mass balance of Meighen Ice Cap. *Atmos.-Ocean*, 17(3):181–199, 1979.

M. Bougamont, J. L. Bamber, and W. Greuell. Development and test of a surface mass balance model for the greenland ice sheet. *J. Geophys. Res.*, 110(F04018), 2005.

D. P. Dee, S. M. Uppala, A. J. Simmons, P. Berrisford, P. Poli, S. Kobayashi, U. Andrae, M. A. Balmaseda, G. Balsamo, P. Bauer, P. Bechtold, A. C. M. Beljaars, L. van de Berg, J. Bidlot, N. Bormann, C. Delsol, R. Dragani, M. Fuentes, A. J. Geer, L. Haimberger, S. B. Healy, H. Hersbach, E. V. Hólm, L. Isaksen, P. Kållberg, M. Köhler, M. Matricardi, A. P. McNally, B. M. Monge-Sanz, J.-J. Morcrette, B.-K. Park, C. Peubey, P. de Rosnay, C. Tavolato, J.-N. Thépaut, and F. Vitart. The ERA-Interim reanalysis: Configuration and performance of the data assimilation system. *Quarterly Journal of the Royal Meteorological Society*, 137(656):553–597, 2011. doi: 10.1002/qj.828.

J. Ettema, M. R. van den Broeke, E. Van Meijgaard, W. J. Van de Berg, J. L. Bamber, J. E. Box, and R. C. Bales. Higher surface mass balance of the Greenland ice sheet revealed by high-resolution climate modeling. *Geophys. Res. Lett.*, 36(L12501), 2009. doi: 10.1029/2009GL038110.

J. Ettema, M. R. van den Broeke, E. van Meijgaard, and W. J. van de Berg. Climate of the Greenland ice sheet using a high-resolution climate model – Part 1: Evaluation. *The Cryosphere*, 4(2):511–527, 2010. doi: 10.5194/tc-4-511-2010.

X. Fettweis, B. Franco, M. Tedesco, J. H. van Angelen, J. T. M. Lenaerts, M. R. van den Broeke, and H. Gallée. Estimating Greenland ice sheet surface mass balance contribution to future sea level rise using the regional atmospheric climate model MAR. *The Cryosphere Discussions*, 6(4):3101–3147, 2012. doi: 10.5194/tcd-6-3101-2012.

M.G. Flanner and C.S. Zender. Linking snowpack microphysics and albedo evolution. *J. Geophys. Res.*, 111(D12208), 2006.

A. S. Gardner, G. Moholdt, B. Wouters, G. J. Wolken, D. O. Burgess, M. J. Sharp, J. G. Cogley, C. Braun, and C. Labine. Sharply increased mass loss from glaciers and ice caps in the Canadian Arctic Archipelago. *Nature*, 473:357–360, 2011. doi: 10.1038/nature10089.

Alex S. Gardner and Martin J. Sharp. A review of snow and ice albedo and the development of a new physically based broadband albedo parameterization. *J. Geophys. Res.*, 115(F1), 03 2010.

P. Kuipers Munneke, M. R. van den Broeke, J. T. M. Lenaerts, M. G. Flanner, A.S. Gardner, and W. J. van de Berg. A new albedo scheme for use in climate models over the Antarctic ice sheet. *J. Geophys. Res.*, 116(D05114), 2011. doi: 10.1029/2010JD015113.

P. Kuipers Munneke, G. Picard, M. R. van den Broeke, J. T. M. Lenaerts, and E. van Meijgaard. Insignificant change in Antarctic snowmelt volume since 1979. *Geophys. Res. Lett.*, 39(L01501), 2012. doi: 10.1029/2011GL050207.

J. T. M. Lenaerts, M. R. van den Broeke, S. J. Déry, E. van Meijgaard, W. J. van de Berg, S. P. Palm, and J. Sanz Rodrigo. Regional climate modeling of drifting snow in Antarctica, Part I: Methods and model evaluation. *J. Geophys. Res.*, 117(D05108), 2012a. doi: 10.1029/2011JD016145.

J. T. M. Lenaerts, M. R. van den Broeke, W. J. van de Berg, E. Van Meijgaard, and P. Kuipers Munneke. A new, high-resolution surface mass balance map of Antarctica (1979-2010) based on regional atmospheric climate modeling. *Geophys. Res. Lett.*, 39(L04501), 2012b. doi: 10.1029/2011GL050713.

R. H. Moss, J. A. Edmonds, K. A. Hibbard, M. R. Manning, S. K. Rose, D. P. van Vuuren, T. R. Carter, S. Emori, M. Kainuma, T. Kram, G. A. Meehl, J. F. B. Mitchell, N. Nakicenovic, K. Riahi, S. J. Smith, R. J. Stouffer, A. M. Thomson, J. P. Weyant, and T. J. Wilbanks. The next generation of scenarios for climate change research and assessment. *Nature*, 463(7282):747–756, 2010. doi: 10.1038/nature08823.

The HadGEM2 Development Team. The HadGEM2 family of Met Office Unified Model climate configurations. *Geoscientific Model Development*, 4(3):723–757, 2011. doi: 10.5194/gmd-4-723-2011.

P. Undén, L. Rontu, H. Järvinen, P. Lynch, J. Calvo, G. Cats, J. Cuxart, K. Eerola, C. Fortelius, J.A.

Garcia-Moya, C. Jones, G. Lenderlink, A. McDonald, R. McGrath, B. Navascues, N. Woetman Nielsen, V. Ødegaard, E. Rodriguez, M. Rummukainen, R. Rõõm, K. Sattler, B. Hansen Sass, H. Savijärvi, B. Wichers Schreur, R. Sigg, H. The, and A. Tijm. HIRLAM-5 Scientific Documentation. Technical report, Swed. Meteorol. and Hydrol. Inst., Norrköping, Sweden, 2002.

S. M. Uppala, P. W. Köllberg, A. J. Simmons, U. Andrae, V. Da Costa Bechtold, M. Fiorino, J. K. Gibson, J. Haseler, A. Hernandez, G. A. Kelly, X. Li, K. Onogi, S. Saarinen, N. Sokka, R. P. Allan, E. Andersson, K. Arpe, M. A. Balmaseda, A. C. M. Beljaars, L. Van De Berg, J. Bidlot, N. Bormann, S. Caires, F. Chevallier, A. Dethof, M. Dragosavac, M. Fisher, M. Fuentes, S. Hagemann, E. Hlm, B. J. Hoskins, L. Isaksen, P. A. E. M. Janssen, R. Jenne, A. P. Mcnally, J.-F. Mahfouf, J.-J. Morcrette, N. A. Rayner, R. W. Saunders, P. Simon, A. Sterl, K. E. Trenberth, A. Untch, D. Vasiljevic, P. Viterbo, and J. Woollen. The ERA-40 re-analysis. *Quarterly Journal of the Royal Meteorological Society*, 131(612): 2961–3012, 2005. doi: 10.1256/qj.04.176.

J. H. Van Angelen, J. T. M. Lenaerts, S. Lhermitte, X. Fettweis, P. Kuipers Munneke, M. R. van den Broeke, and E. van Meijgaard. Sensitivity of Greenland Ice Sheet surface mass balance to surface albedo parameterization: A study with a regional climate model. The Cryosphere, in press, 2012.

E. Van Meijgaard, L. H. van Ulft, W. J. Van de Berg, F. C. Bosvelt, B. J. J. M. Van den Hurk, G. Lenderink, and A. P. Siebesma. The KNMI regional atmospheric model RACMO version 2.1. Technical Report 302, KNMI, De Bilt, The Netherlands, 2008.

P.W. White. Physical processes (CY23R4). Technical report, European Centre for Medium-Range Weather Forecasts (ECMWF), 2001.

B. Wouters, D. Chambers, and E. J. O. Schrama. GRACE observes small-scale mass loss in Greenland. *Geophys. Res. Lett.*, 35(20), 10 2008.

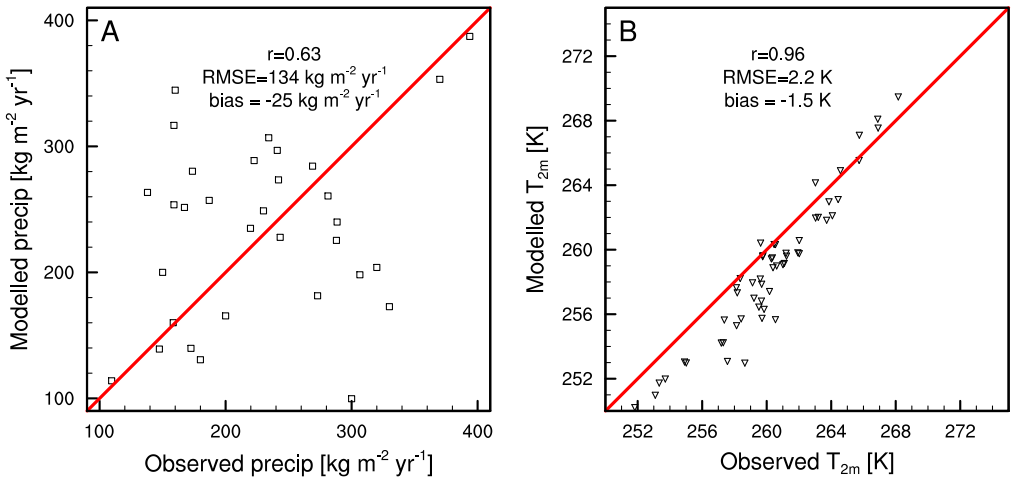

Figure S1: Comparison of modeled vs. observed precipitation (A) and near-surface temperature [corrected for elevation, (B)] for available observations in NCAA. Precipitation is shown as a mean of the overlapping years. The near-surface temperature is observed at daily resolution, and the observations and model values shown here are the means of the overlapping days. See text for more details.

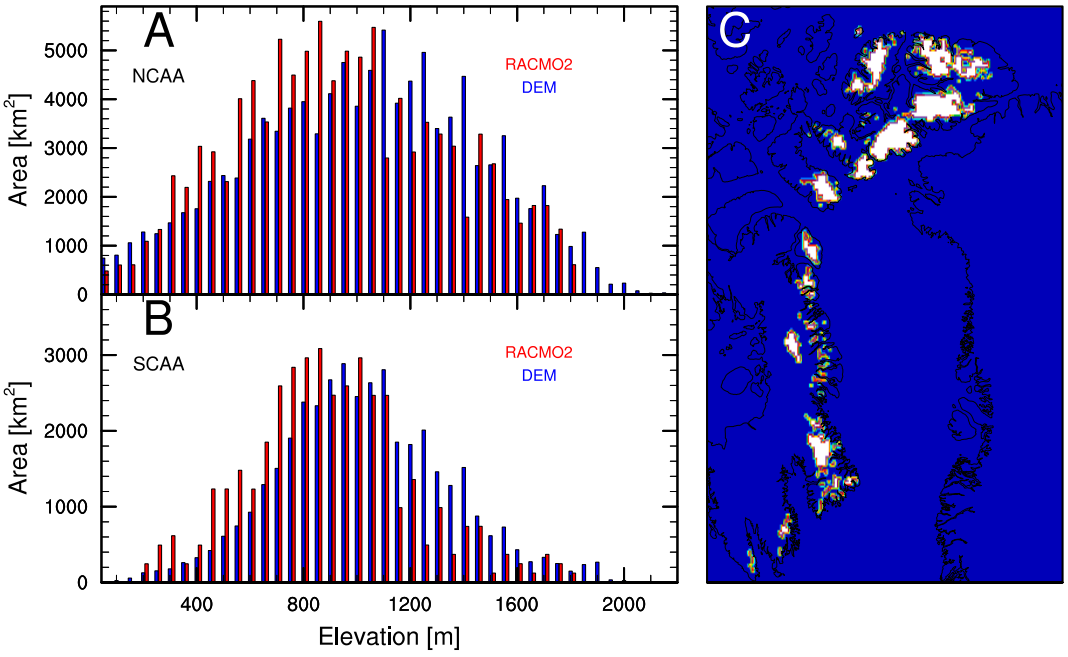

Figure S2: Hypsometry comparison between RACMO2 (red) and high-resolution DEM (blue, Gardner et al. (2011)) (A and B) and RACMO2 ice mask (C). The glaciated surface area is 105000 km^2 for NCAA and 40800 km^2 for SCAA, which is in agreement with the area outlined by Gardner et al. (2011).

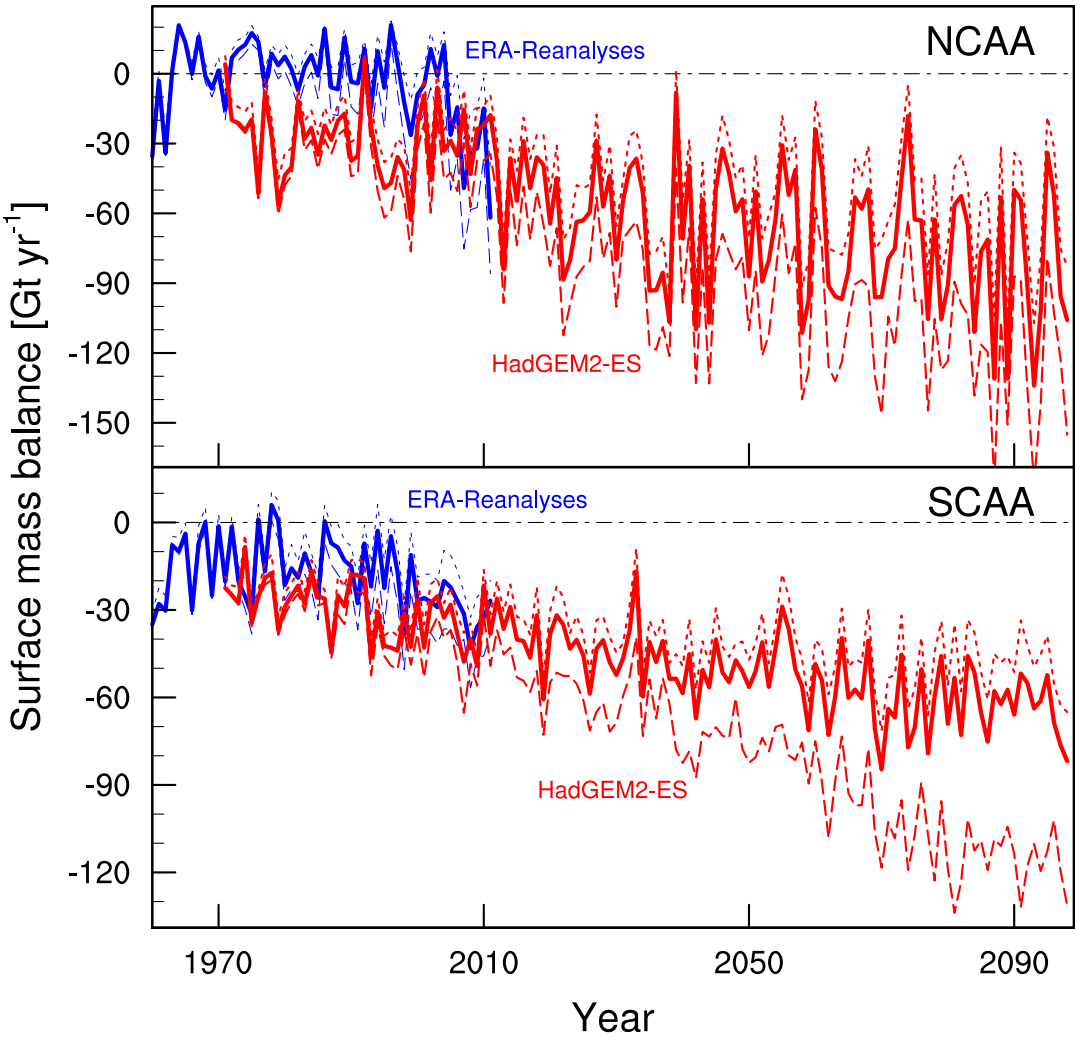

Figure S3: Modelled surface mass balance from RACMO2, forced by ERA-Interim (blue) and HadGEM2-ES (red) for NCAA and SCAA. The full line represents the SMB (corrected for hypsometry), the dashed line shows the SMB sensitivity tests, considering a decrease in ice thickness and associated lower elevation (assuming $\rho_{ice} = 917\ kg\,m^{-3}$), and the dotted line shows SMB including a linearly decreasing glaciated area towards -10% at the end of the simulation.

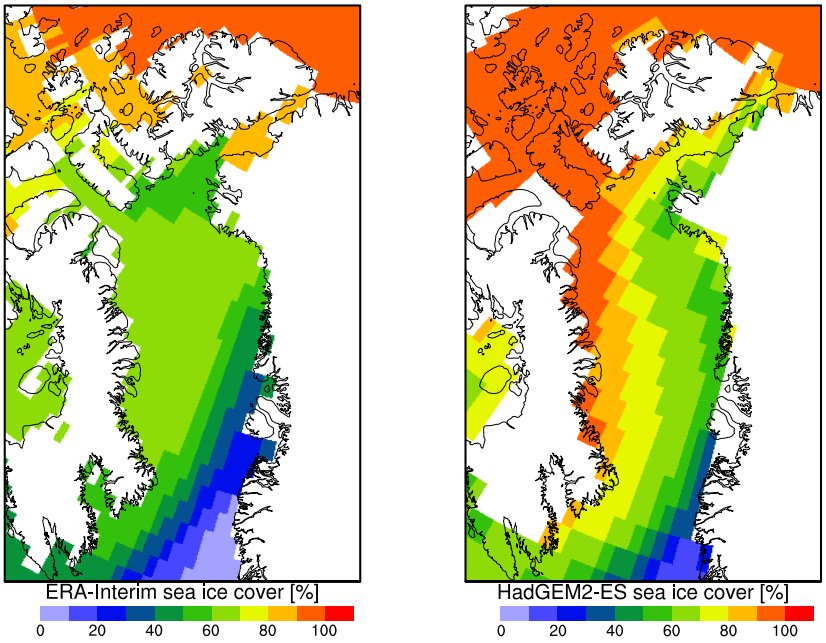

Figure S4: Comparison of present-day sea ice cover in ERA-Interim (left) and historical HadGEM2-ES (right) for the overlapping period (1979-2004).

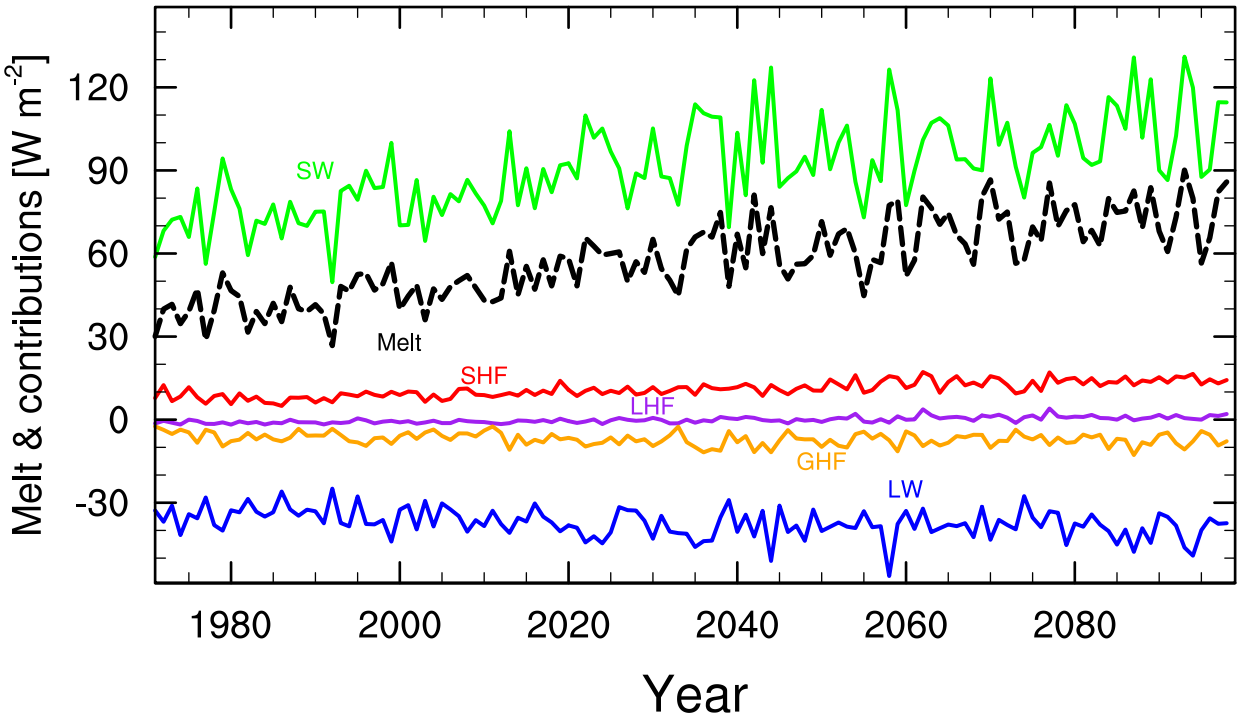

Figure S5: Average CAA melt flux (black) and surface energy balance contributions to melt (SW = shortwave radiation, SHF = sensible heat flux, LHF = latent heat flux, GHF = ground heat flux, and LW = longwave radiation) according to RACMO2 forced by HadGEM2-ES (1971-2098).

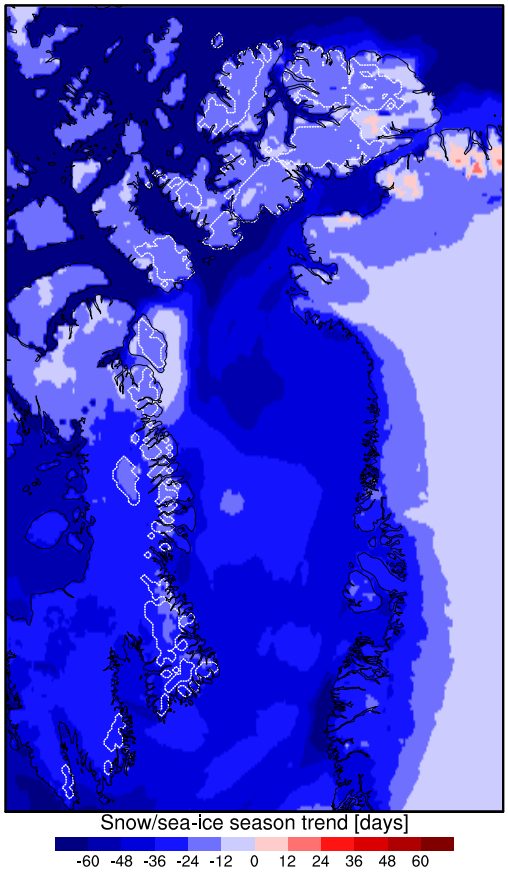

Figure S6: Trend (1971-2098, in days) in snow-covered season (land) and sea-ice covered season (ocean) in RACMO2 forced with HadGEM2-ES.

Table S1: SMB and its components (in Gt yr^{-1}) from RACMO2, forced by ERA-Interim (first two columns, mean of period 1971-2000 and 2000-2011, respectively) and by HADGEM2-ES (last three columns, mean of period 1971-2000, 2000-2011 and 2080-2098), respectively. Sublimation is negligible (<1 Gt yr^{-1}), and is not shown. The last row shows the SMB after hypsometry correction.

	ERA-40 and ERA-Interim		HadGEM2-ES		
	1971-2000	2000-2011	1971-2000	2000-2011	2080-2098
Precipitation	49±6	48±6	40±4	47±5	55±8
Snowfall	41±4	38±5	30±3	36±5	36±6
Rainfall	8±2	10±2	9±2	12±2	19±3
Melt	94±20	129±25	126±23	137±14	223±28
Runoff	69±20	106±25	108±24	119±15	214±29
Refreezing	33±2	33±3	28±3	30±2	29±3
SMB	-22±20	-59±28	-69±23	-71±15	-158±33
SMB Corrected	-13±18	-48±26	-58±22	-60±15	-144±33